Supporting Information

Enhanced Neutral Seawater Splitting on Less-Defective, Two-Dimensional $LaTiO_2N$ Photoanodes Prepared from Layered Perovskite $BaLa_4Ti_4O_{15}$

Thanh Tam Thi Tran and Jeongsuk Seo*

Department of Chemistry, College of Natural Sciences, Chonnam National University, 77 Yongbong-ro, Buk-gu, Gwangju 61186, Republic of Korea

*Corresponding author.

E-mail address: j_seo@chonnam.ac.kr (J. Seo).

Table S1. Comparison of a present work with previously reported results for syntheses of $LaTiO_2N$ particles and the resulting water splitting activities in neutral electrolytes.

Target	Synthesis method	Electrode preparation	Cocatalyst	Light source	Electrolyte (pH)	Photocurrent at 1.23 V_{RHE}	Year	Reference
$LaTiO_2N$ transformed from $BaLa_4Ti_4O_{15}$	Flux-assisted calcination	Spin coating	$Co(OH)_x$	AM 1.5G	0.5 M NaCl (pH 6.4)	2.4 mA cm^{-2}	2024	This work
			-			0.17 mA cm^{-2}		
$LaTiO_2N$ transformed from $NaLaTiO_4$	Molten salt assisted solid-state reactions	Electrophoretic deposition	-	Xe lamp ($\lambda \geq 420$ nm)	0.1 M K_3PO_4/K_2HPO_4 (pH 7.95)	ca. 600 μA cm^{-2}	2024	[1]
$LaTi_{0.9}Mg_{0.1}O_{2y+1}N_{1-y}$	Polymerized complex method	Drop casting	-	Xe lamp ($\lambda \geq 420$ nm)	Na_2SO_4 (pH 7)	ca. 350 μA cm^{-2}	2023	[2]
$LaTiO_2N$:TiN	Phase-pure powder-product	Spin coating	-	QTH* lamp, 250 W output	0.1 M Na_2SO_4 aqueous solution (pH 7)	ca. 0.5 μA cm^{-2}	2022	[3]
Ba modified $LaTiO_2N$	Polymerized complex method	Electrophoretic deposition	-	AM 1.5G	0.1 M Na_2SO_4 (pH 7)	ca. 50 μA cm^{-2}	2020	[4]

*QTH: Quartz Tungsten Halogen

References

[1] Wang, R.; He, H.; Shi, L.; Du, D.; Lin, G.; Zhang, C.; Xu, X., Unleashing Photocarrier Transport in Mesoporous Single-Crystalline $LaTiO_2N$ for High-Efficiency Photocatalytic Water Splitting. *Adv. Energy Mater.* **2024,** *14* (6), 2302996.

[2] Lin, G.; Sun, X.; Xu, X., Mg modified $LaTiO_2N$ with ameliorated photocarrier separation for solar water splitting. *Appl. Catal. B: Environ.* **2023,** *324*, 122258.

[3] Hojamberdiev, M.; Mora-Hernandez, J. M.; Vargas, R.; Heppke, E. M.; Yubuta, K.; Yamakata, A.; Kadirova, Z.; Torres-Martínez, L.; Teshima, K.; Lerch, M., Eliciting the contribution of TiN to photoelectrochemical performance enhancement of Imma-$LaTiO_2N$ at neutral pH. *Mater. Today Energy* **2022,** *27*, 101053.

[4] Lin, G.; Xu, X., Ba-Modified $LaTiO_2N$ as an Efficient Visible Light Active Photocatalyst for Water Oxidation. *ACS Sustain. Chem. Eng.* **2020,** *8* (26), 9641-9649.

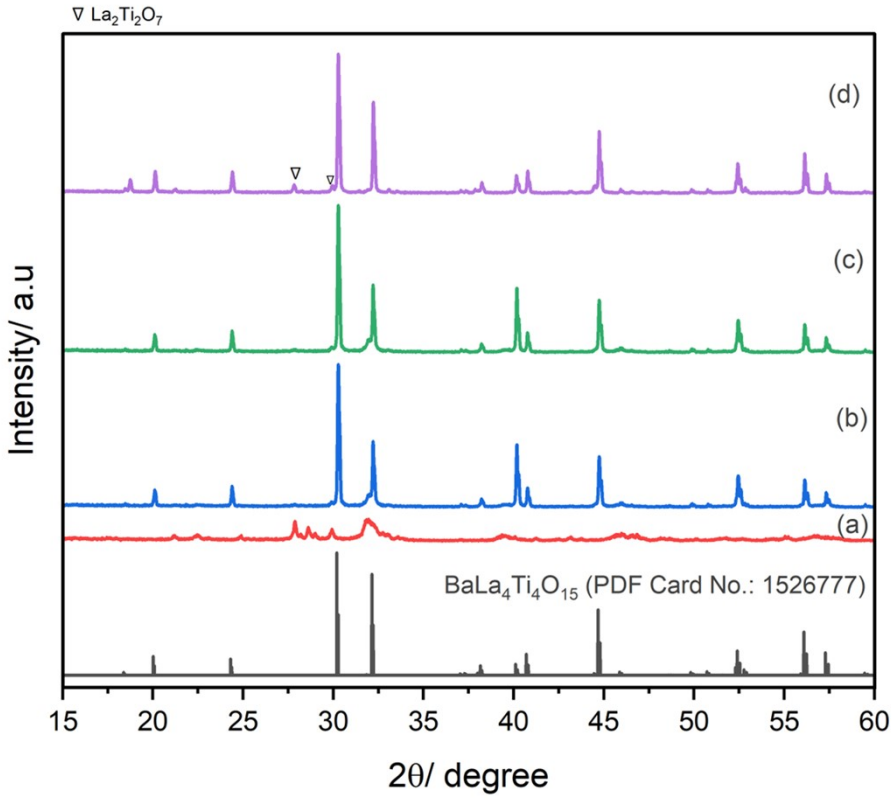

Figure S1. XRD patterns for $BaLa_4Ti_4O_{15}$ prepared via flux-assisted calcination at different temperatures of (a) 1173, (b) 1273, (c) 1373, and (d) 1473 K for 20 h and subsequent washing by distilled water.

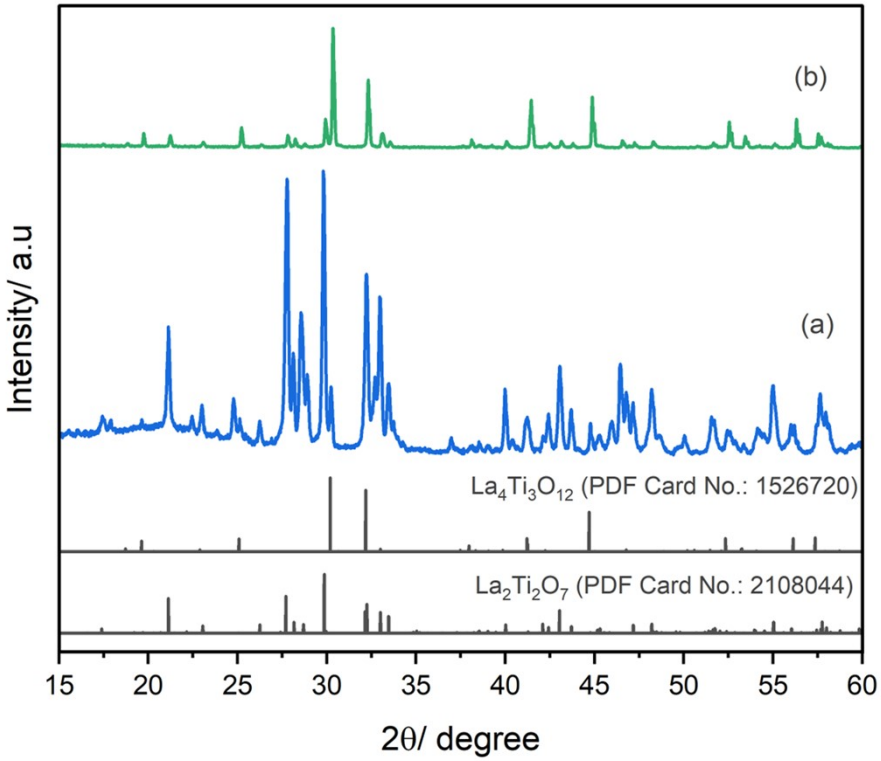

Figure S2. XRD patterns for $La_5Ti_4O_x$ prepared via flux-assisted calcination at different temperatures of (a) 1273 and (b) 1373 K for 20 h and subsequent washing by distilled water.

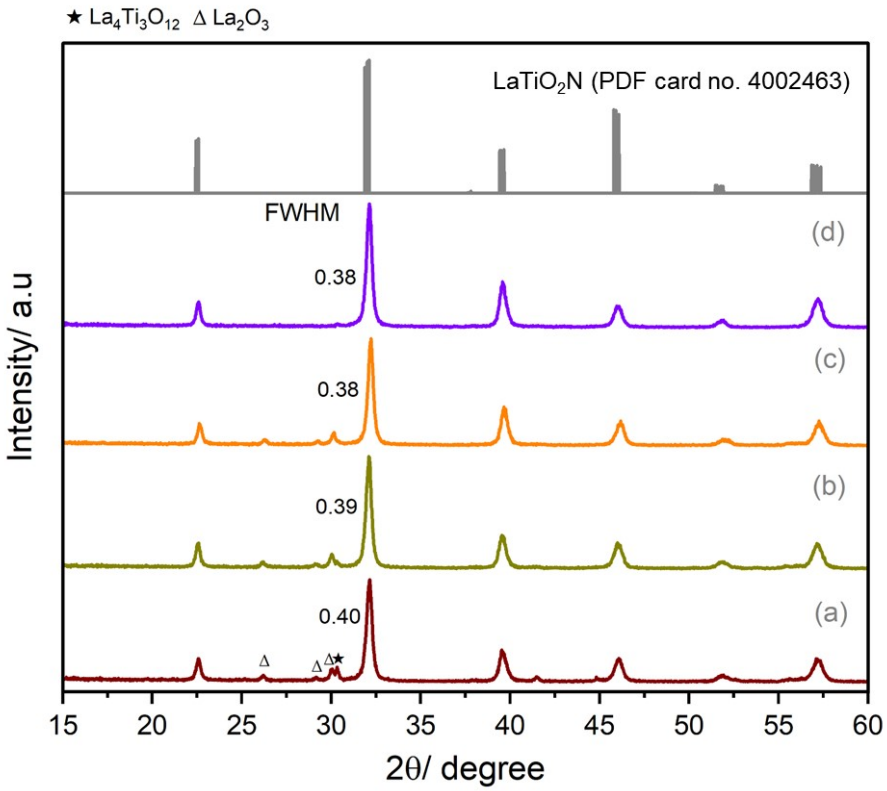

Figure S3. XRD patterns for $LaTiO_2N$ prepared by nitridation of $La_5Ti_4O_x$ at 1123 K for (a) 30, (b) 40, and (c) 50 h and (d) after subsequent acid treatment.

Table S2. Elemental compositions of $LaTiO_2N$ prepared by nitridation of layered perovskite oxides, namely, (a) $La_2Ti_2O_7$, (b) $BaLa_4Ti_4O_{15}$, and (c) $La_5Ti_4O_x$, at 1123 K for 20 h and subsequent acid treatment, which were determined by ICP-MS analysis with an error range of 0.5%.

	Elemental composition		
	Ba/Ti	La/Ti	K/Ti
$La_2Ti_2O_7$	-	0.99	0.00_4
$BaLa_4Ti_4O_{15}$	0.18	0.89	n.d.
$La_5Ti_4O_x$	-	1.24	0.00_4

Figure S4. pH determination of the waste water resulted from the washing of $LaTiO_2N$, as-prepared by nitridation of $BaLa_4Ti_4O_{15}$, with deionized water. The washing procedure in 500 mL of deionized water for 1 h was repeated five times. The pH values measured after each washing were compared with that of deionized water (last photo).

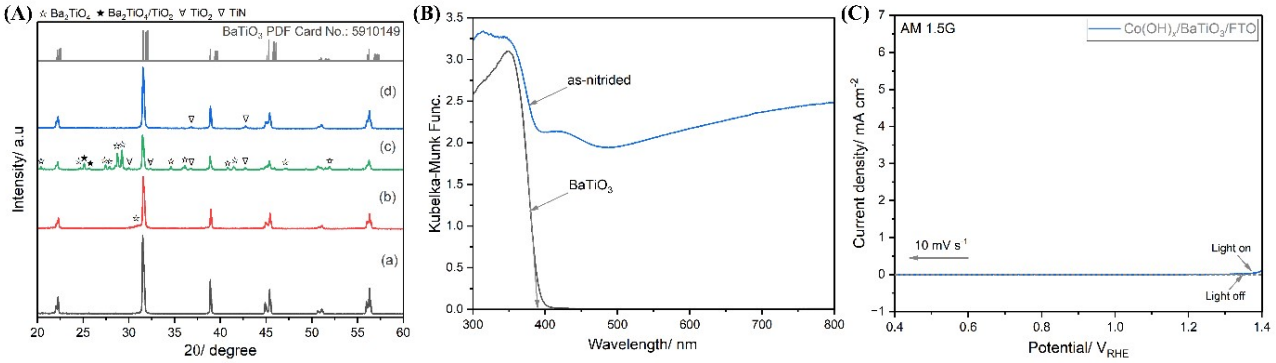

Figure S5. (A) XRD patterns for (a) $BaTiO_3$ and corresponding derivatives prepared by nitridation at 1123 K for (b) 10 and (c) 20 h and (d) after acid treatment. Single-crystalline $BaTiO_3$ was synthesized by flux-assisted calcination of $BaCO_3$−TiO_2 mixture at 1273 K for 20 h. $BaTiO_3$ remained even after nitridation for 20 h, accompanied by TiN impurity traces. (B) DRS spectra of $BaTiO_3$ and corresponding derivative prepared by nitridation at 1123 K for 20 h. The TiN impurity led to the light absorption of visible light. (C) LSV data for $Co(OH)_x/BaTiO_3$/FTO photoanodes during seawater splitting under chopped AM 1.5 G simulated sunlight in 0.5 M NaCl electrolyte buffered with 0.2 M KPi at pH 6.4. In the photoanode, $BaTiO_3$ indicates the derivative prepared by nitridation at 1123 K for 20 h and after acid treatment.

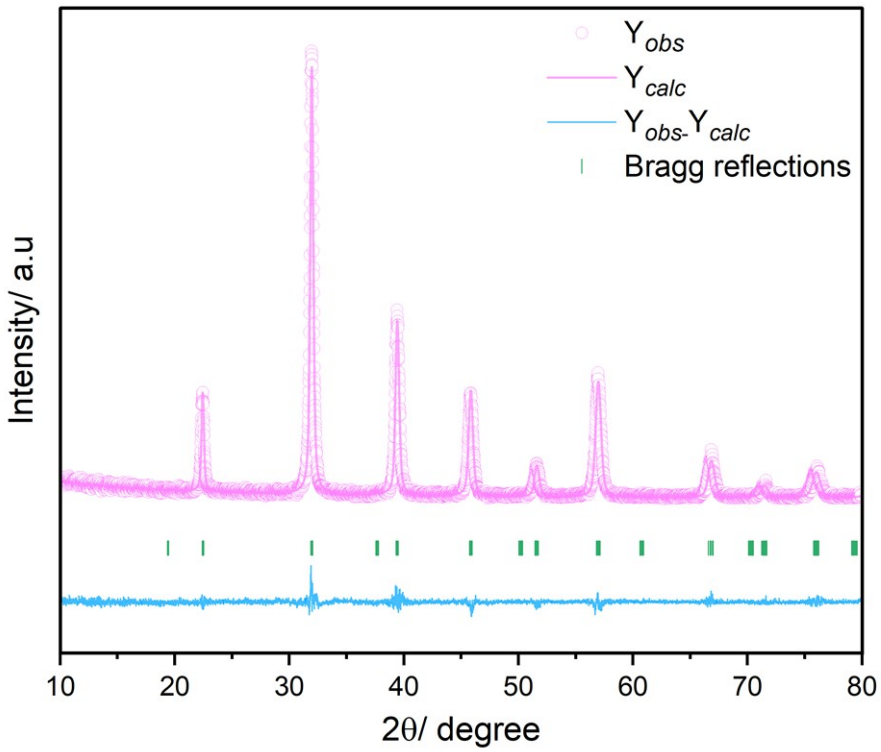

Figure S6. XRD patterns for Rietveld refinement of $LaTiO_2N$ prepared by nitridation of $BaLa_4Ti_4O_{15}$ at 1123 K for 20 h and after subsequent acid treatment. Dotted and solid curves represent observed and calculated patterns, respectively. Differences between patterns are shown at the bottom. Reliability factors were summarized in Table S2.

Table S3. Rietveld refinement results using XRD patterns for $LaTiO_2N$ prepared by the nitridation of layered perovskite $BaLa_4Ti_4O_{15}$ at 1123 K for 20 h and subsequent acid treatment. Background and profile fitting were determined by B-spline and split pseudo-Voigt functions, respectively. During the refinements, constraints are that same atomic coordinates and temperature factors was set, and total occupancy was specified (1.000).

	$LaTiO_2N$
Structure type	Perovskite
R_{wp} (%)	20.5
R_p (%)	16.6
R_{exp}	6.65
R_{Bragg}	6.099
χ^2	9.50
crystal system	orthorhombic
space group	*I-1*
a (Å)	5.596629
b (Å)	7.914129
c (Å)	5.613168
α (°)	89.991
β (°)	89.972
γ (°)	89.981
volume (Å^3)	269.944
Z	4
Radiation	Cu$K\alpha$ radiation
Wavelength, Å	λ_1= 1.540590, λ_2= 1.544310

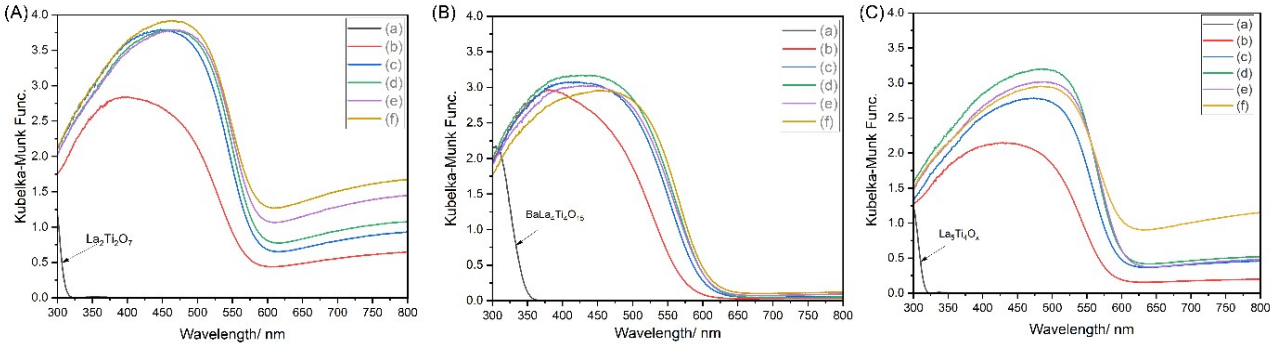

Figure S7. UV-Vis DRS spectra of $LaTiO_2N$ and intermediate derivatives during nitridation of (A) $La_2Ti_2O_7$ (B) $BaLa_4Ti_4O_{15}$, and (C) $La_5Ti_4O_x$ at 1123 K for (a) 0, (b) 1, (c) 5, (d) 10, and (e) 20 h (50 h in the case of $La_5Ti_4O_x$) and (f) after subsequent acid treatment.

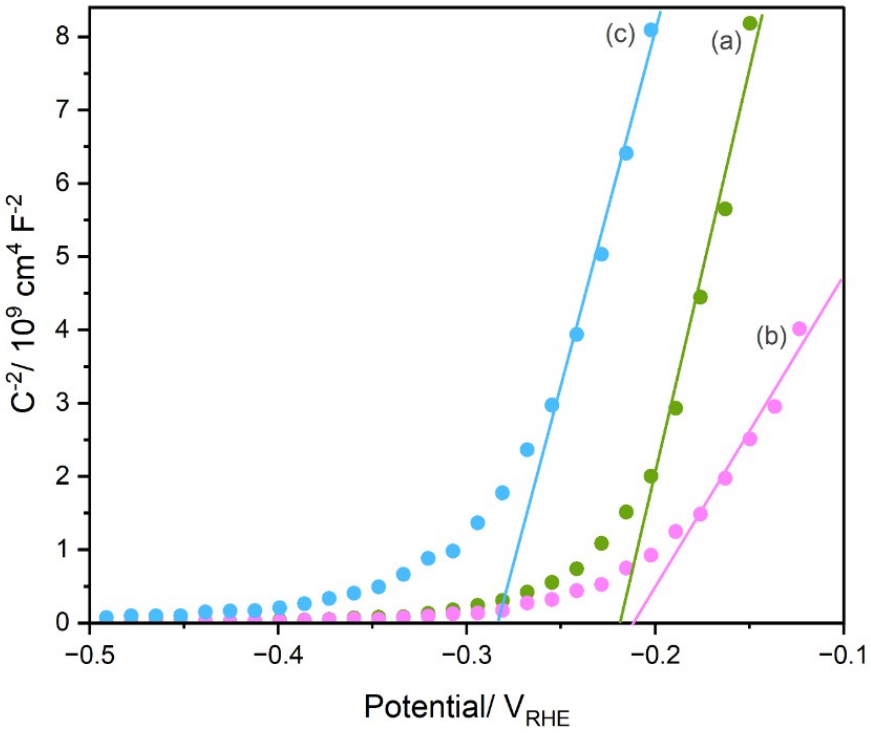

Figure S8. Mott-Schottky plots at a frequency of 1 kHz for bare $LaTiO_2N$/FTO photoanodes prepared by nitridation of (a) $La_2Ti_2O_7$, (b) $BaLa_4Ti_4O_{15}$, and (c) $La_5Ti_4O_x$ synthesized by flux-assisted calcination. The measurements were performed in an Ar-saturated 0.5 M NaCl electrolyte buffered with 0.2 M KPi at pH 6.4 under dark conditions.

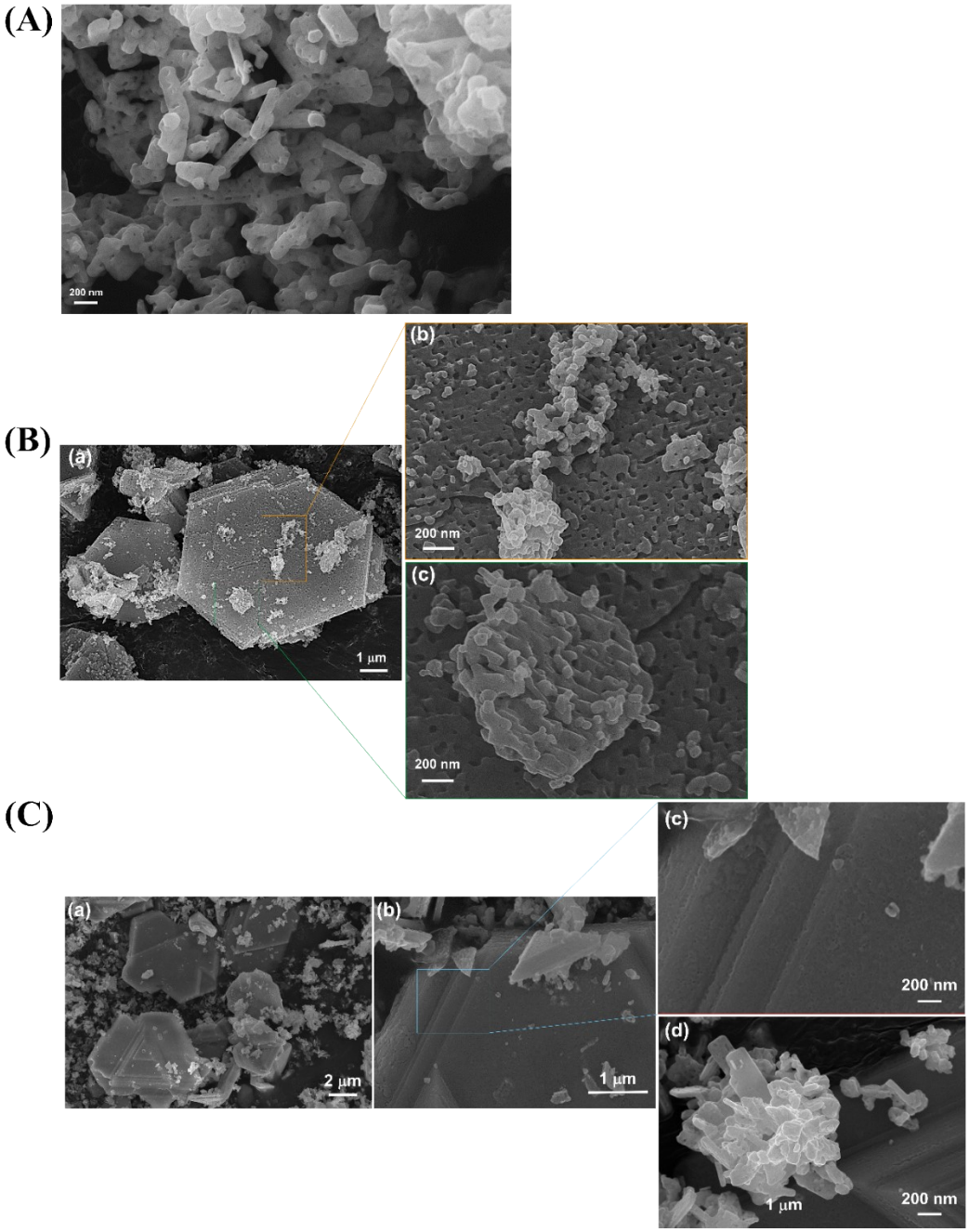

Figure S9. SEM images of $LaTiO_2N$ particles prepared by nitridation of (A) $La_2Ti_2O_7$, (B) $BaLa_4Ti_4O_{15}$, and (C) $La_5Ti_4O_x$ at 1123 K for 20 h (50 h in the case of $La_5Ti_4O_x$).

Table S4. BET surface areas of $LaTiO_2N$ prepared by nitridation of layered perovskite oxides, namely, (a) $La_2Ti_2O_7$, (b) $BaLa_4Ti_4O_{15}$, and (c) $La_5Ti_4O_x$, at 1123 K for 20 h (50 h in the case of $La_5Ti_4O_x$) and subsequent acid treatment.

	BET surface area /m^2 g^{-1}
(a) $La_2Ti_2O_7$	14.0
(b) $BaLa_4Ti_4O_{15}$	16.3
(c) $La_5Ti_4O_x$	12.8

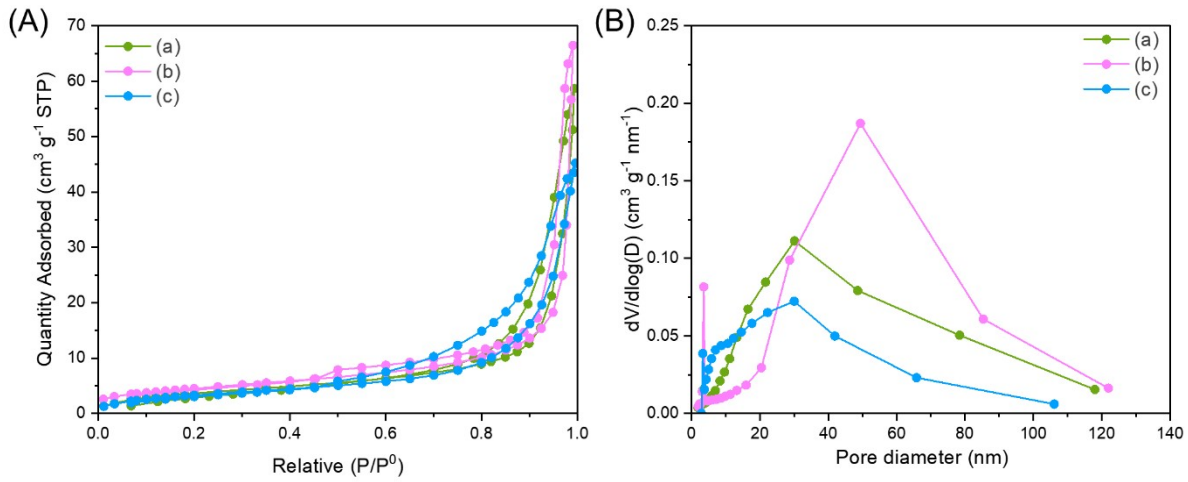

Figure S10. (A) N_2 adsorption-desorption isotherms at 77 K and (B) pore size distributions in $LaTiO_2N$ prepared by nitridation of layered perovskite oxides, namely, (a) $La_2Ti_2O_7$, (b) $BaLa_4Ti_4O_{15}$, and (c) $La_5Ti_4O_x$, at 1123 K for 20 h (50 h in the case of $La_5Ti_4O_x$) and subsequent acid treatment. The pore size distributions were deduced from the N_2 desorption isotherms using BJH procedures.

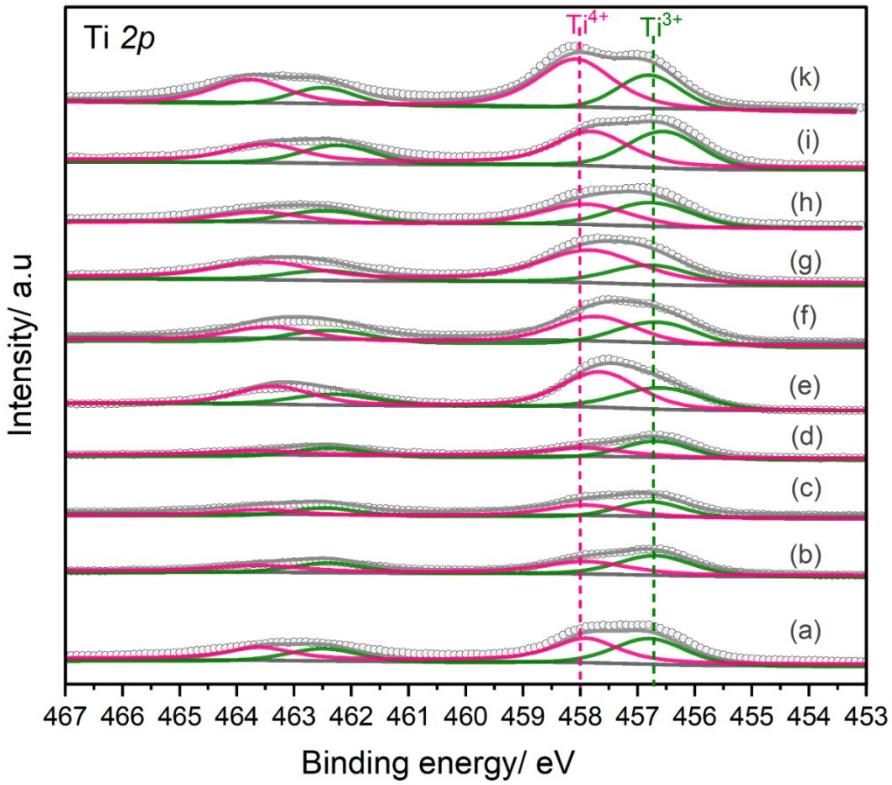

Figure S11. Narrow-scan Ti 2p XPS spectra acquired on $LaTiO_2N$ surfaces prepared by nitridation of $La_2Ti_2O_7$ for (a) 5 and (b) 10 h, $La_5Ti_4O_x$ for (c) 5 and (d) 50 h, $BaLa_4Ti_4O_{15}$ for (e) 1, (f) 5, (g) 10, (h) 15, and (i) 20 h and (k) after subsequent acid nitridation. All the nitridation were carried out at 1123 K.

Table S5. Surface cation defects on $LaTiO_2N$ surfaces prepared by nitridation of $La_2Ti_2O_7$ for (a) 5 and (b) 10 h, $La_5Ti_4O_x$ for (c) 5 and (d) 50 h, $BaLa_4Ti_4O_{15}$ for (e) 1, (f) 5, (g) 10, (h) 15, and (i) 20 h and (k) after subsequent acid nitridation. All the nitridation were carried out at 1123 K. The surface fractions were estimated based on the narrow-scan Ti 2p XPS spectra in Figure S11.

	Fractions of surface Ti species	
	Ti^{4+}/Ti_{total}	Ti^{3+}/Ti_{total}
(a) $La_2Ti_2O_7$−5 h	0.46	0.54
(b) $La_2Ti_2O_7$−10 h	0.39	0.61
(c) $La_5Ti_4O_x$−5 h	0.53	0.47
(d) $La_5Ti_4O_x$−50 h	0.45	0.55
(e) $BaLa_4Ti_4O_{15}$−1 h	0.63	0.37
(f) $BaLa_4Ti_4O_{15}$−5 h	0.56	0.44
(g) $BaLa_4Ti_4O_{15}$−10 h	0.65	0.35
(h) $BaLa_4Ti_4O_{15}$−15 h	0.53	0.47
(i) $BaLa_4Ti_4O_{15}$−20 h	0.50	0.50
(k) $BaLa_4Ti_4O_{15}$−acid	0.69	0.31

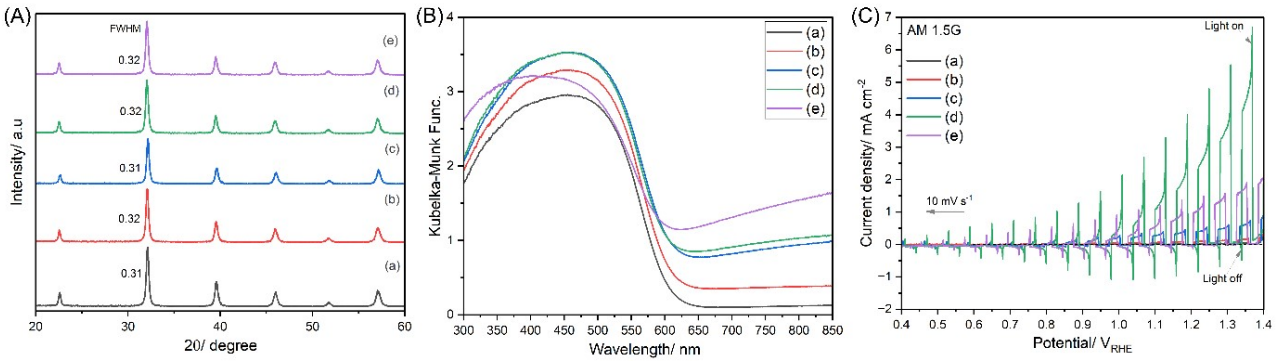

Figure S12. (A) XRD patterns and (B) UV-Vis DRS spectra for $LaTiO_2N$ particles prepared by nitridation of $BaLa_4Ti_4O_{15}$ at 1123 K for 20 h, followed by acid treatment (a) as-prepared and subsequent annealing in Ar flow at different temperature (b) 873, (c) 923, (d) 973, and (e) 1073 K for 1 h. and (C) LSV data for the corresponding $Co(OH)_x/LaTiO_2N$/FTO photoanodes during seawater splitting in 0.5 M NaCl electrolyte buffered with 0.2 M KPi at pH 6.4 under chopped AM 1.5 G simulated sunlight.

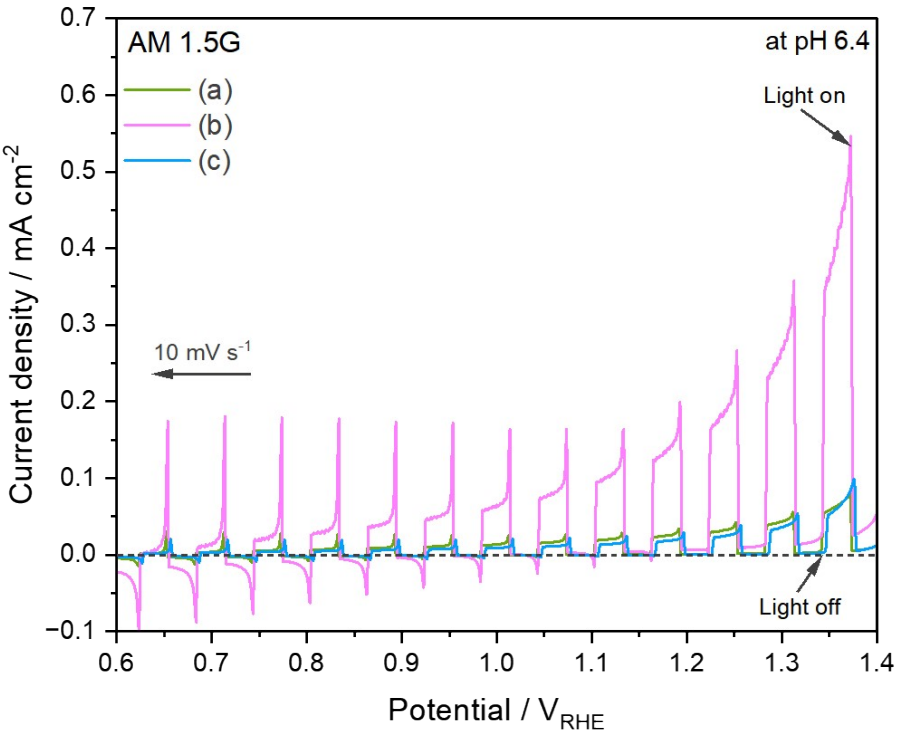

Figure S13. LSV curves acquired on bare $LaTiO_2N$/FTO photoanodes prepared by the nitridation of different layered perovskites, namely, (a) $La_2Ti_2O_7$, (b) $BaLa_4Ti_4O_{15}$, and (c) $La_5Ti_4O_x$, at 1123 K for 20 h and subsequent annealing in Ar flow at 973 K for 1 h, during seawater splitting under chopped AM 1.5G simulated sunlight. All curves were acquired by sweeping the potential from 1.4 to 0.6 V_{RHE} at a scan rate of 10 mVs^{-1} in an Ar-saturated 0.5-M NaCl aqueous solution buffered with 0.2-M KPi at pH 6.4.

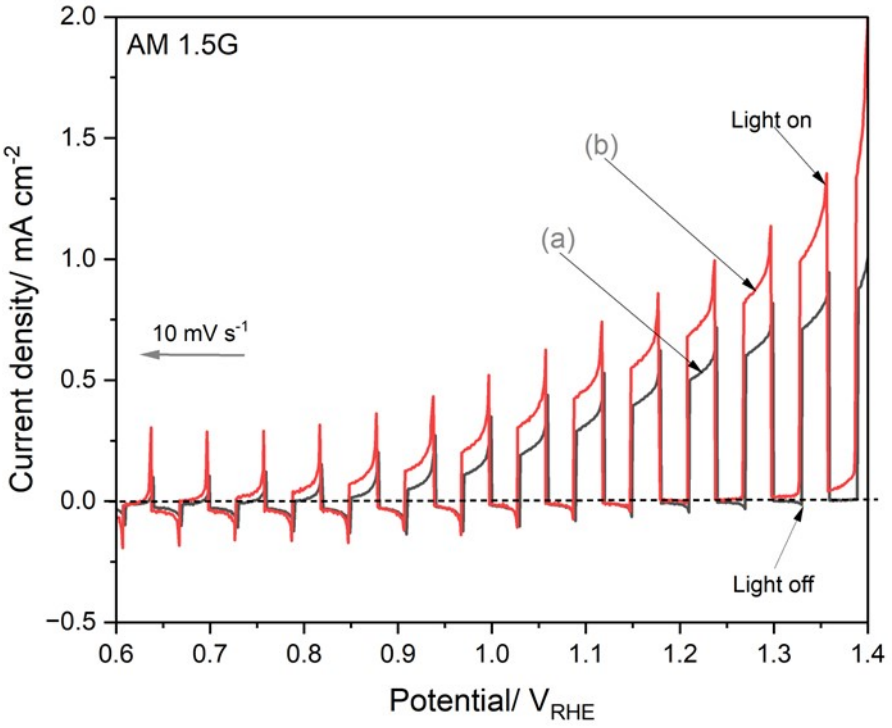

Figure S14. LSV data for the $Co(OH)_x/LaTiO_2N$/FTO photoanodes, nitrided from $La_5Ti_4O_x$ at 1123 K for (a) 20, and (b) 50 h and followed by acid treatment and subsequent annealing in Ar flow at 973 K for 1 h, during seawater splitting in 0.5 M NaCl electrolyte buffered with 0.2 M KPi at pH 6.4 under chopped AM 1.5 G simulated sunlight.

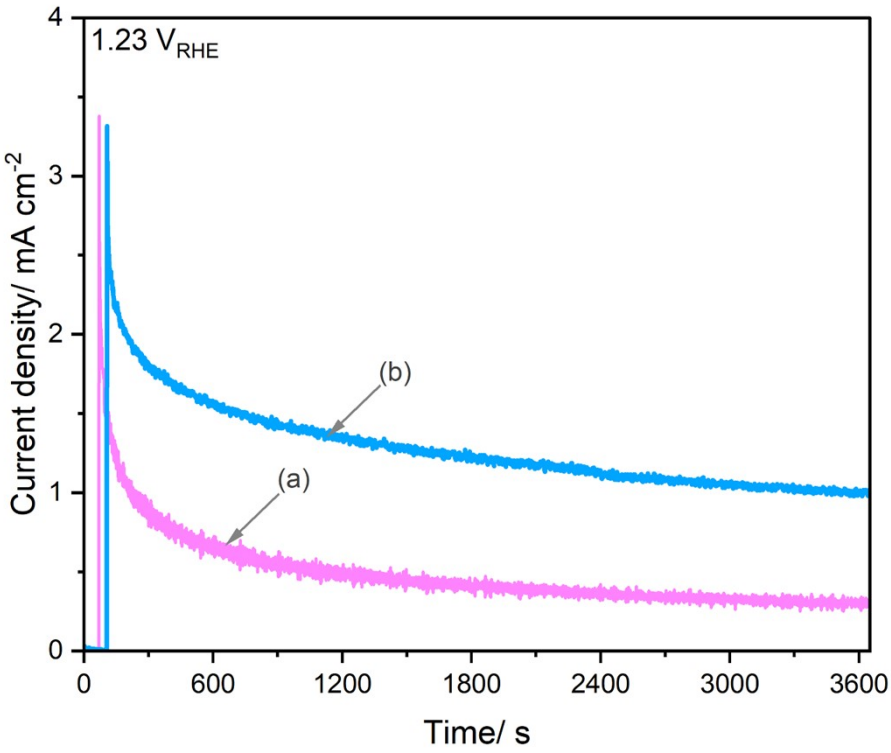

Figure S15. Chronoamperometry curves acquired using $Co(OH)_x/LaTiO_2N$/FTO photoanodes, prepared by nitridation of $BaLa_4Ti_4O_{15}$ at 1123 K for 20 h, during seawater splitting at an applied potential of 1.23 V_{RHE} for 1 h under chopped AM 1.5 G simulated sunlight in stirred Ar-saturated 0.5 M NaCl aqueous electrolytes buffered with 0.2 M KPi at (a) pH 6.4 and (b) 13.

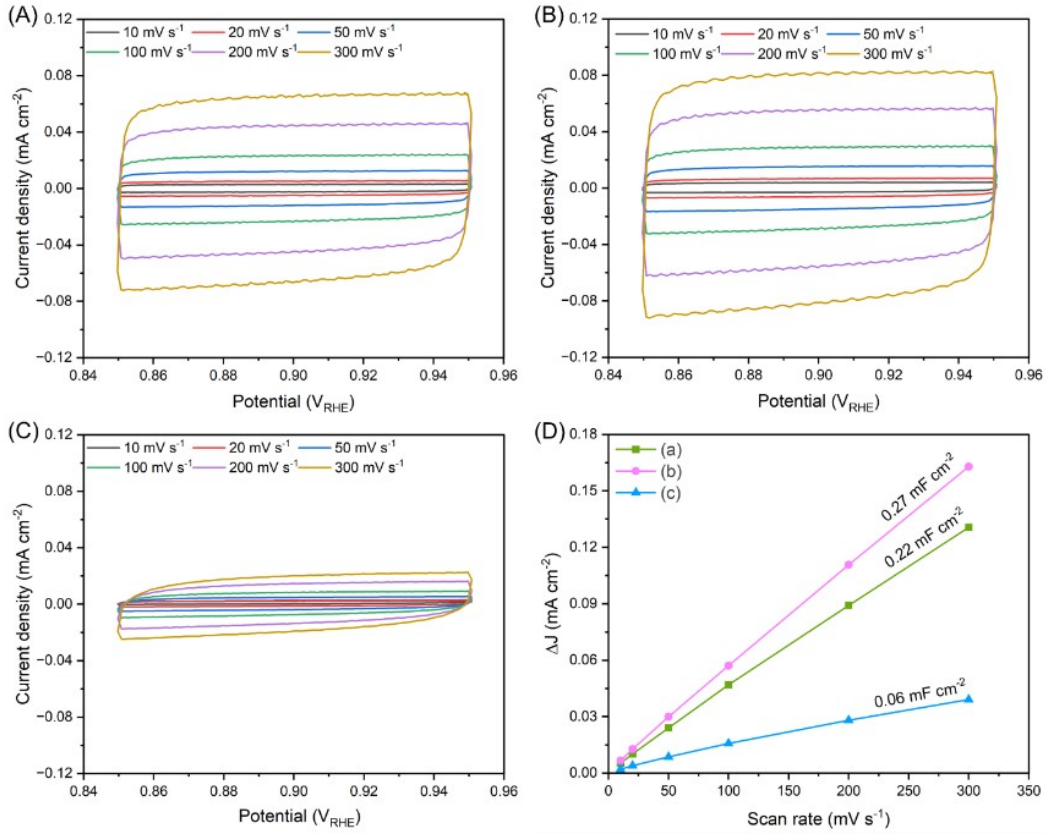

Figure S16. Cyclic voltammograms of $Co(OH)_x/LaTiO_2N$/FTO photoanodes prepared from (A) $La_2Ti_2O_7$, (B) $BaLa_4Ti_4O_{15}$, and (C) $La_5Ti_4O_x$, measured in a stirred Ar-saturated 0.5-M NaCl buffered with 0.2-M KPi at pH 6.4 in the potential range of 0.9±0.05 V_{RHE} at different scan rates of 10, 20, 50, 100, 200 and 300 mV s^{-1} in darkness and (D) Charging current density difference ($\Delta J = J_a - J_c$) between the anodic current (J_a) and cathodic current (J_c) of the corresponding $Co(OH)_x/LaTiO_2N$/FTO photoanodes measured in the potential range of 0.9±0.05 V_{RHE} versus scan rates (v). Double-layer capacitance (C_{dl}) values, i.e., halves of the linear slopes of ΔJ-v plots, are provided for each photoanode.

Table S6. The EIS fitting results of $Co(OH)_x$/$LaTiO_2N$/FTO photoanodes, nitrided from (a) $La_2Ti_2O_7$, (b) $BaLa_4Ti_4O_{15}$, and (c) $La_5Ti_4O_x$ synthesized by flux-assisted calcination. The EIS measurements were performed in a stirred Ar-saturated 0.5 M NaCl aqueous electrolyte buffered with 0.2 M KPi at pH 6.4 under AM 1.5G simulated irradiation at the applied potential of 1.23 V_{RHE}.

	R_1 (kΩ)	CPE1-T*; Q ($\Omega^{-1}s^n$)	CPE1-P*; n	R_2 (kΩ)	CPE2-T*; Q ($\Omega^{-1}s^n$)	CPE2-P*; n	R_3 (kΩ)
(a)$La_2Ti_2O_7$	0.024	1.0×10^{-4}	0.75	4.4	9.8×10^{-5}	0.95	0.40
(b)$BaLa_4Ti_4O_{15}$	0.029	1.0×10^{-4}	0.79	0.67	9.8×10^{-5}	0.95	0.10
(c)$La_5Ti_4O_x$	0.026	1.0×10^{-4}	0.80	4.8	9.9×10^{-5}	0.90	0.50

*CPE-T and CPE-P refer to the constant phase element parameters, amplitude and value range, respectively.

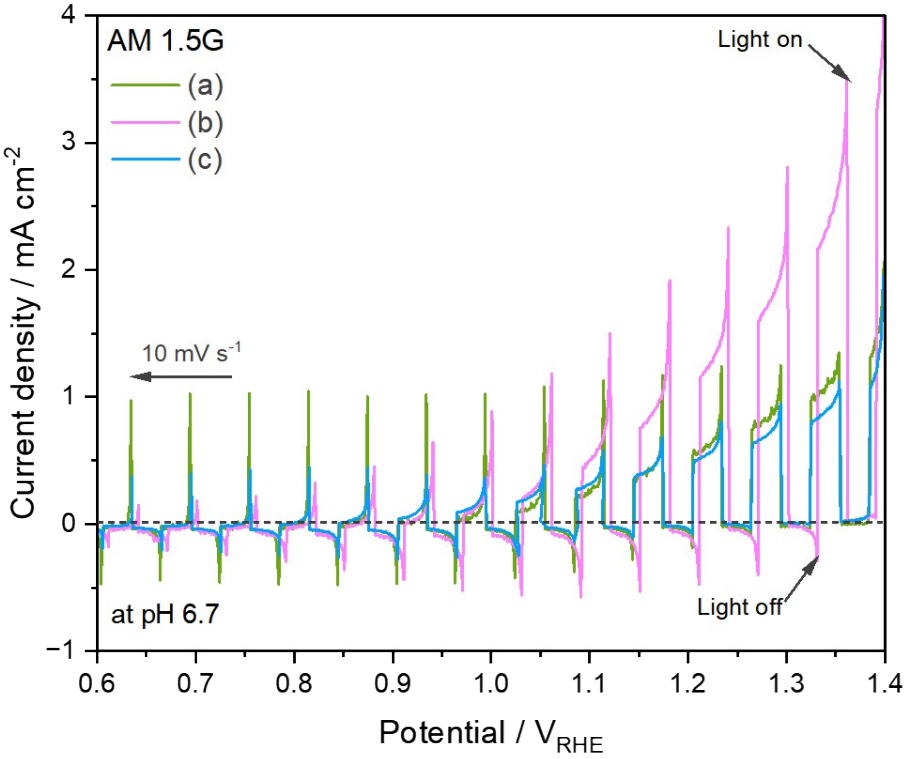

Figure S17. LSV data for $Co(OH)_x$/$LaTiO_2N$/FTO photoanodes prepared by nitridation of different layered perovskite oxides, (a) $La_2Ti_2O_7$, (b) $BaLa_4Ti_4O_{15}$, and (c) $La_5Ti_4O_x$, during water splitting at pH 6.7 under chopped AM 1.5G simulated sunlight. All photoelectrochemical data were acquired by sweeping the potential from 1.4 to 0.6 V_{RHE} at a scan rate of 10 mVs^{-1} in an Ar-saturated 0.2 M KPi aqueous electrolyte.

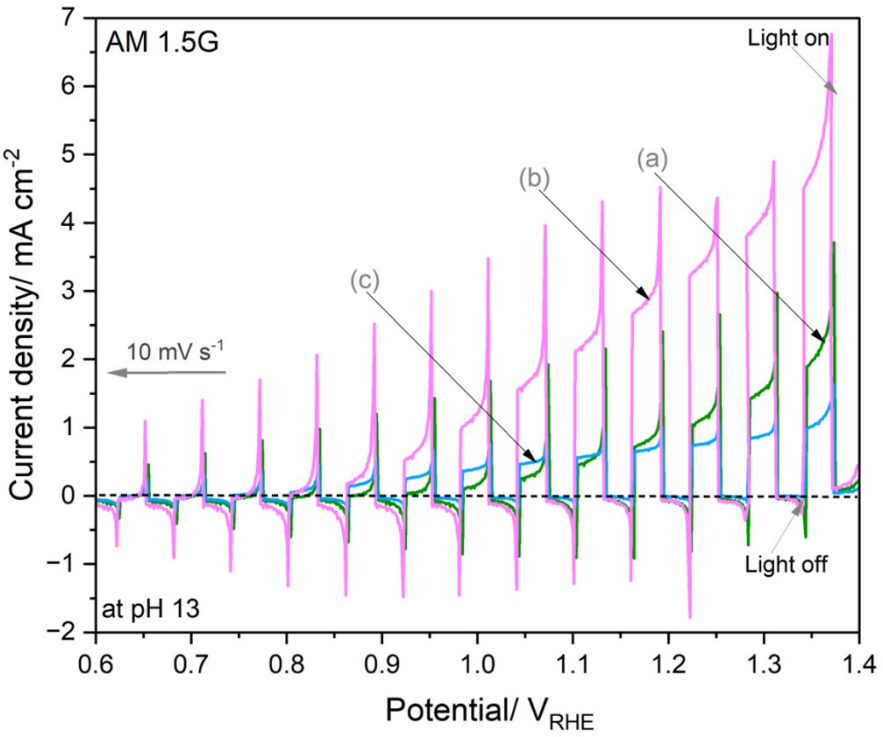

Figure S18. LSV data for $Co(OH)_x/LaTiO_2N$/FTO photoanodes prepared by nitridation of different layered perovskite oxides, (a) $La_2Ti_2O_7$, (b) $BaLa_4Ti_4O_{15}$, and (c) $La_5Ti_4O_x$, during seawater splitting at pH 13 under chopped AM 1.5G simulated sunlight. All photoelectrochemical data were acquired by sweeping the potential from 1.4 to 0.6 V_{RHE} at a scan rate of 10 mVs^{-1} in an Ar-saturated 0.5 M NaCl aqueous electrolyte buffered with 0.2 M KPi adjusted to pH 13.

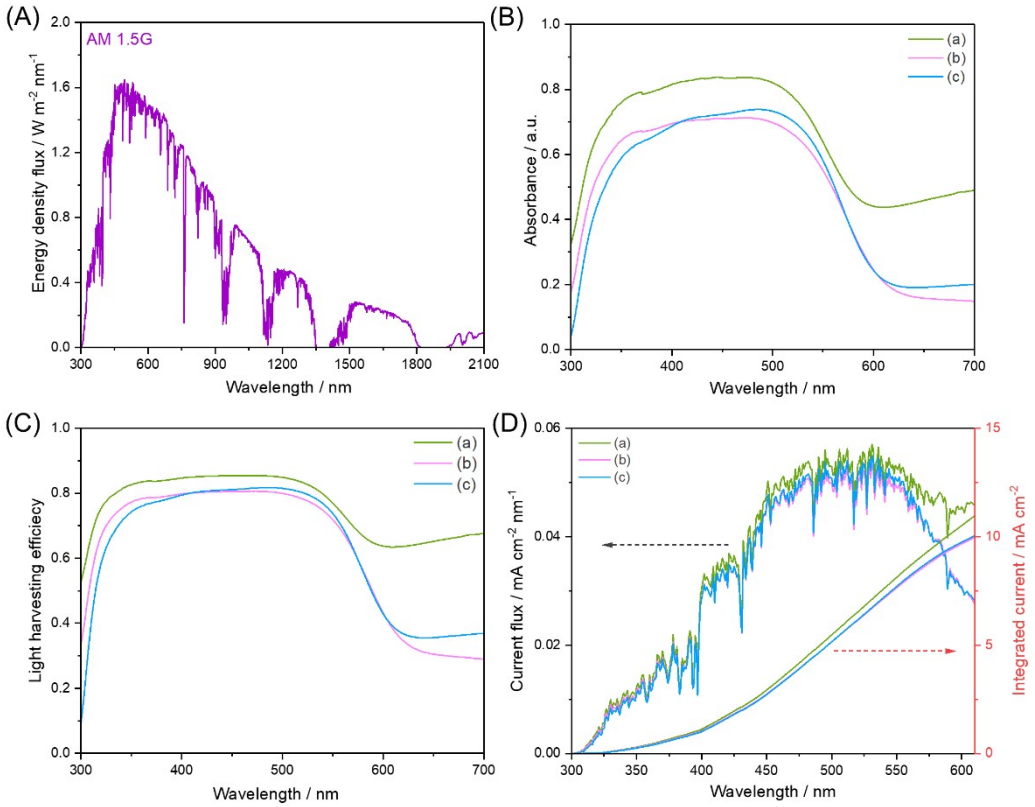

Figure S19. (A) Energy density flux for the standard solar spectrum (AM 1.5 Global). (B) Absorbance, (C) light harvesting efficiency (LHE) spectra, and (D) calculated current density flux and integrated current density for $LaTiO_2N$/FTO photoanodes prepared by nitridation of different layered perovskite oxides, (a) $La_2Ti_2O_7$, (b) $BaLa_4Ti_4O_{15}$, and (c) $La_5Ti_4O_x$. According to DRS spectra result, the light absorption wavelength edge of the oxynitride photoanodes was estimated at 610 nm, leading to photon absorption rate J_{abs} of 11.0, 10.0, and 10.0 mA cm^{-2}, respectively.